

## Intercomparison of wave-driven current models

P. Péchon <sup>a,\*</sup>, F. Rivero <sup>b</sup>, H. Johnson <sup>c</sup>, T. Chesher <sup>d</sup>,  
B. O'Connor <sup>e</sup>, J.-M. Tanguy <sup>f</sup>, T. Karambas <sup>g</sup>, M. Mory <sup>h</sup>,  
L. Hamm <sup>i</sup>

<sup>a</sup> *Laboratoire National d'Hydraulique, EDF, Chatou, France*

<sup>b</sup> *Laboratori d'Enginyeria Marítima, UPC, Barcelona, Spain*

<sup>c</sup> *Danish Hydraulic Institute, Horsholm, Denmark*

<sup>d</sup> *HR Wallingford, Wallingford, UK*

<sup>e</sup> *University of Liverpool, Liverpool, UK*

<sup>f</sup> *Serv. Techn. Central des Ports Maritimes et des Voies Navig., Compiègne, France*

<sup>g</sup> *Aristotle University of Thessaloniki, Thessaloniki, Greece*

<sup>h</sup> *Laboratoire des Écoulements Géophysiques et Industriels, Grenoble, France*

<sup>i</sup> *SOGREAH, Grenoble, France*

Received 2 April 1996; accepted 20 December 1996

---

### Abstract

Seven numerical models which simulate waves and currents in the surf-zone are tested for the case of a reduced-scale detached breakwater subjected to the action of regular waves with normal incidence. The computed wave heights, water levels and velocities are compared with measurements collected in an experimental wave basin. The wave height decay in the surf-zone is predicted reasonably well. Set-up and currents appear to be less well predicted. This intercomparison exercise shows that radiation stresses are systematically overestimated by formulations used in the models, mean bottom shear stresses are not always co-linear with the mean bottom velocity vector in shallow water, and turbulence modelling in the surf-zone requires a sophisticated model. © 1997 Elsevier Science B.V.

*Keywords:* Numerical models; Breaking waves; Nearshore currents; Radiation stress; Breakwater

---

### 1. Introduction

Wave-driven currents generated in the surf-zone can be very intense and they can be responsible for severe morphological changes in the coastal area. Their influence spreads often beyond the surf-zone by the generation of associated rip-currents. So accurate

---

\* Corresponding author.

prediction of these currents is essential in many coastal engineering projects. In the surf-zone, currents are often three-dimensional but important features can be understood with modelling concepts based on fewer dimensions. The appropriate model depends mainly on the complexity of the problem, on the type of the beach and on the balance between accuracy and computation efficiency.

The distribution of longshore currents in the cross-shore profile has been formulated by Putnam et al. (1949), Brün (1963), Eagleson (1965), and Bowen (1969) in the case of an infinite rectilinear beach with constant bottom slope. The original analysis of Longuet Higgins (1970) established the relationship between the gradient of the radiation stress for waves arriving obliquely to the shore line and the resulting longshore currents. A solution was found for a planar beach. Then his theory was the basis of a range of numerical models such as:

— cross-shore profile models, which give the longshore current distribution ignoring longshore variation, by Southgate (1989),

— two-dimensional coastal area models, based on depth-averaged current modules, made by many authors such as Ebersole and Dalrymple (1979), Wu and Liu (1982), Wind and Vreugdenhil (1986), and most of the authors of the present paper whose models are described hereafter,

— three-dimensional or quasi-three-dimensional coastal area models developed by de Vriend and Stive (1987), Sanchez-Arcilla et al. (1992), and Péc'hon and Teisson (1995).

This paper attempts to evaluate the performance of seven coastal area models versus a common physical model data set for the case of a detached breakwater. The models described herein comprise either depth-averaged 2D or 3D flow solvers, which all determine the (stationary) hydrodynamic field as a result of wave forcing. By these means all are suitable for coastal applications where the time scale associated with the two horizontal dimensions cannot be separated, such as that due to the complex flow field around structures or topography, or due to complicated driving forces, e.g. river outflows. The effect of wave-driven currents on morphodynamics is not taken up here but is presented in a companion paper by Nicholson et al. (1997).

The models are all based on the same structure which comprises three main elements. The first element defines the wave conditions at the offshore model limit, as well as the bathymetric domain over which these waves will propagate. The second element describes how the waves are modified as they propagate inshore, and the third element describes how the specific wave fields drive flow circulations within the model domain. The level of complexity of each model varies, with some models including feedback loops to account for the modification of the waves as a result of the general circulation pattern caused by such a wave field. Clearly, in these cases some iteration is required in order to generate stationary wave-driven currents.

In the following sections, each participating institute's model is described in terms of its component parts. The physical model set-up and test programme are then outlined, and each models' performance versus this data set is assessed. Finally, conclusions and recommendations from this intercomparison exercise are drawn.

The wave and current models will be hereinafter referred to as:

- W1 and C1 for ARTEMIS and TELEMAR-3D developed by EDF-LNH, France,
- W2 and C2 for PROPS and CIRCO developed by LIM-UPC, Spain,

- W3 and C3 for MIKE 21 PMS and MIKE 21 HD developed by DHI, Denmark,
- W4 and C4 for FDWAVE and TIDEFLOW-2D developed by HR Wallingford Ltd, UK,
- W5 and C5 developed by the Maritime Group at the University of Liverpool, UK,
- W6 and C6 developed by STCPMVN, France,
- W7 and C7 developed by Aristotle University of Thessaloniki, Greece.

In the following presentations of models, only parts used in the test case are described.

## 2. Description of the numerical models

### 2.1. The wave models

#### 2.1.1. The equations

All the wave models used in the intercomparison exercise reproduce refraction, shoaling, diffraction and breaking phenomena. However, the equations are slightly different and can be divided into three types:

— Models W1, W3 and W6 are based on the mild-slope equation (Berkhoff, 1972). W1 and W6 solve the complete equation while W3 solves the parabolic approximation to the equation using the method of Kirby (1986) which significantly increases the range of allowable wave angles.

— Models W2, W4 and W5 compute wave incidence from the irrotationality condition of the wave number vector combined with the eikonal equation originally put forward by Battjes (1968) and extended by Yoo and O'Connor (1986) and Rivero and Arcilla (1993). Wave height is found from the wave action conservation principle. In W5, weak non-linear effects are included by allowing for the influence of the water depth on the wave amplitude.

— Model W7 solves the hyperbolic time-dependent linear equations of Copeland (1985a) without stating the assumption of progressive waves.

#### 2.1.2. Inclusion of the breaking effect

Energy dissipation due to breaking waves is assumed to be similar to the dissipation in a bore (Lamb, 1932). It is expressed in W3 and W4 by the formulation proposed by Battjes and Janssen (1978). This method is based on a Rayleigh distribution of wave heights truncated at a local breaker height and the fraction of broken waves is introduced. The following test is conducted with regular waves, so this parameter is set to 0 or 1 since all the waves at a given location are either breaking or non-breaking.

In W5, energy dissipation is based on energy excess using a criterion for breaker height based on the Iribarren number (Yoo and O'Connor, 1988a)

In W2, because of the regular wave condition, it is preferable to use the formulation of Dally et al. (1985). The rate of dissipation of broken wave energy is proportional to the difference between the actual energy flux and a lower stable flux level.

A dispersion term is introduced into the time-dependent momentum equation of W7. It is proportional to a horizontal eddy viscosity coefficient estimated from the solution of the turbulent kinetic energy equation (Karambas and Koutitas, 1992).

In W1 and W6, according to the schematised geometry investigated hereafter, a simple procedure is used assuming that the ratio of wave height to still water depth is constant in the surf-zone and equal to 0.8.

Wave–current interaction is accounted for in W2 and W5.

Table 1 summarises the wave model characteristics.

## 2.2. The wave-driven current models

The current models are based on time-averaged equations. To establish the equations, the velocity is separated into three contributions: the unknown time-averaged velocity, the purely periodic current corresponding to wave motion and turbulent fluctuations. The Navier–Stokes equations are then averaged over time (Svendsen and Lorentz, 1989) which lead to another set of 3D equations, and can also be integrated over the water depth (Longuet Higgins, 1970) giving 2D horizontal equations. The flow models C2 to C7 solve the vertically-integrated equations whereas C1 solves the three-dimensional equations.

The orbital velocities of waves generate driving forces via radiation stress gradients. The turbulent fluctuations of velocity create mixing of momentum. The velocity reduction in the near-bed boundary layer induces bottom shear stresses. The modelling of these three contributions are detailed hereafter for each model.

### 2.2.1. The driving terms

The gradient of radiation stresses which drives currents is expressed in terms of the energy dissipation of breaking waves in C1, C4 and C5 following Dingemans et al. (1987). The required wave incidence for C4 and C5 comes from the solution of wave number irrotationality in the wave model. For model C1, the computed instantaneous wave velocity resulting from the mild-slope equation follows an ellipse and therefore there is not simple incidence. In this case, the wave incidence is supposed to be given by the large axis of the ellipse.

In C1 the vertical profile of the driving force increases near the surface due to drag from the roller (Péchon and Teisson, 1995). Moreover, in this model the driving terms are corrected by a coefficient 0.7; this correction is discussed in Section 4.2.

In C2, C3 and C6 the radiation stresses are calculated using the classical expression of Longuet Higgins (1970), and the gradients are deduced.

In C2 the correlation between the horizontal and vertical wave velocity components is calculated according to Rivero and Arcilla (1995) whereas other models neglect this term.

In C7 radiation stresses are derived without the assumption of progressive waves according to Copeland (1985b).

### 2.2.2. Mixing of momentum

All the current models use the eddy viscosity concept. In C4 and C5 the eddy viscosity coefficient is expressed in terms of the dissipation rate of total energy due to bed friction and breaking (Battjes, 1975). The diffusion coefficient in C1 depends also

Table 1  
Wave models

Equations	Breaking effect	Wave-current interaction
W1 mild slope equations	criterion in the surf-zone, wave height/water depth = 0.8 energy dissipation given by Dally et al. (1985)	no
W2 irrotational wave number, eikonal equation, wave action conservation		yes
W3 parabolic mild slope equations, method of Kirby	energy dissipation given by Battjes and Janssen (1978) modified for regular waves	no
W4 irrotational wave number, eikonal equation, wave action conservation	energy dissipation given by Battjes and Janssen (1978) modified for regular waves	no
W5 irrotational wave number, eikonal equation, wave action conservation	energy dissipation based on energy excess using a criterion for wave height	yes
W6 mild slope equations	criterion in the surf-zone, wave height/water depth = 0.8 dispersion term	no
W7 hyperbolic time-dependent equations		no

Table 2  
Current models

Driving force	Viscosity coefficient	Bottom friction
C1 energy dissipation formulation, three-dimensional	constant + wave energy dissipation kinetic energy equation	quadratic law of WDV
C2 gradients of radiation stresses, vertical–horizontal correlation		quadratic law of WDV + orbital velocity
C3 gradients of radiation stresses	constant	quadratic law of WDV
C4 energy dissipation formulation	energy dissipation of wave and bottom friction	quadratic law of WDV
C5 energy dissipation formulation	energy dissipation of wave and bottom friction	quadratic law of WDV
C6 gradients of radiation stresses	constant	quadratic law of WDV + orbital velocity
C7 without the assumption of progressive waves	kinetic energy equation	quadratic law of WDV

WDV = wave-driven velocity.

on the wave energy dissipation of breaking waves but a minimum value is specified because of the low values found behind the structure.

In C3 the viscosity coefficient is constant and close to the values used in the other models in the present application.

In C2 and C7 the viscosity coefficient is expressed in terms of the turbulent kinetic energy (t.k.e.). A transport equation is used to calculate t.k.e., which accounts for the combined effect of advection, diffusion, production due to wave energy dissipation and shear flow, and dissipation of t.k.e.

### 2.2.3. Bottom friction

The formulations of bottom friction used in the models are a quadratic law of the wave-driven velocity (C1, C3, C4, C5, C6, C7), or the wave-driven velocity plus orbital velocity (C2).

In all the models the friction coefficient is enhanced by wave effects according to various methods (C1: Soulsby et al., 1993; C2: Swart, 1974; C3: Fredsoe, 1984; C4 and C5: Yoo and O'Connor, 1988b; C6: Nishimura, 1982). The difficulty is to have a law which is valid over a large range of wave conditions, from small wave heights behind the structure to large ones in the open area. C7 uses the Chezy formula and each component of the bottom stress is increased by the effect of the same component of the maximum orbital velocity according to Bijker (1967). It follows that the bottom stress and the wave-driven velocity vectors are not co-linear.

Table 2 summarises the current model characteristics.

## 3. The test case

Mory and Hamm (1997) measured currents behind a detached breakwater in a wave tank. An intercomparison of the numerical models on the same reduced scale case has been performed.

The horizontal dimensions of the wave basin are 30 m by 30 m. The bed consists of three parts (Fig. 1):

- a horizontal bed in the offshore region. This part is 4.4 m wide and 0.33 m deep,
- an underwater plane beach with a slope of 1:50 between  $-0.33$  m and 0.0 m (still water level),
- an emerged plane beach with a slope of 1:20, cresting at  $+0.066$  m.

A half detached breakwater 6.66 m long and 0.87 m wide is built parallel to the shoreline. The off-shore side of the structure is low-reflective and the onshore side is a vertical wall. The lateral sides of the tank are also vertical walls, so they are reflective.

Several wave conditions were tested in the experimental basin, but only one is selected here for which an extensive set of measurements is available. Reference should be made to the original paper for a more detailed insight on measurements. In the present test the generated wave is regular. The wave height at the wave maker is 7.5 cm, the period is 1.7 s and the incidence is normal to the shoreline.

Breaking line location, wave height, set-up and velocity fields were measured in the basin. The numerical results will be compared with these data in Section 4.

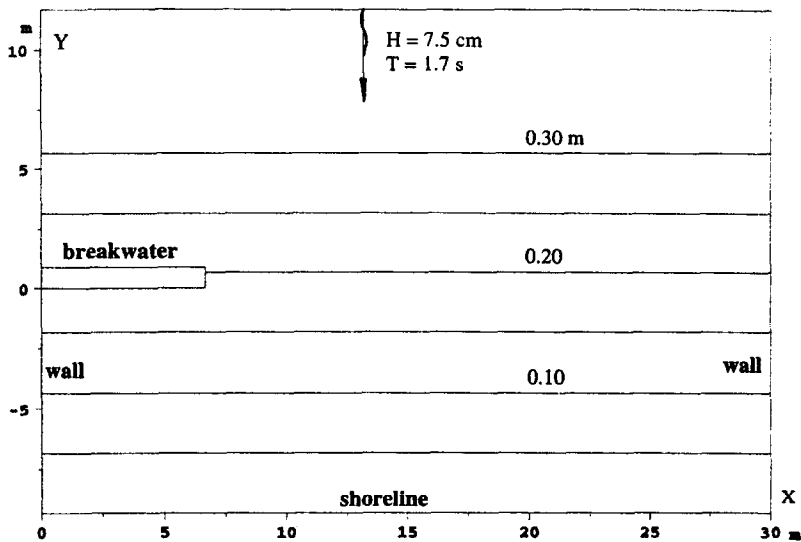


Fig. 1. The test case, bathymetry contour lines.

basin. The numerical results will be compared with these data in Section 4.

In a wave tank, long-period oscillations may occur because of boundary reflections, particularly for regular waves. So a special attention was taken on the calculation of time-averaged measured velocity by using a long sequence of recording. Moreover, it was seen that such oscillations were not generated in the present case.

The coordinate system referred to in the following is indicated in Fig. 1. The  $OX$  axis is parallel to the breakwater and the  $OY$  axis is oriented toward the wave maker. The origin of the coordinate system is at the junction of the breakwater and the side-wall of the basin.

There are differences between field and reduced scale model. For instance, the energy of air bubbles in breaking waves is transferred into turbulent motion generated by uprising bubbles and scale effects may be expected in this aspect. It was not possible to avoid these problems in the physical model. However to reduce these effects and to have a fully turbulent bottom shearstress, the bottom of the tank was made of rough concrete.

## 4. Intercomparison of results

### 4.1. The wave field

The wave refracts on the plane beach, diffracts behind the detached breakwater and breaks in shallow water. The location of the breaking line visualised in the experimental basin is contained in Fig. 2. In the open area it is located between  $y = -3.0$  and  $-5.0$  m and moves shoreward to  $-6.0$  m behind the structure. The computed breaking lines outside the lee of the structure are in the range of variation of the observed data, except for the breaking line of W7 which is slightly too much offshore. In the lee of the breakwater, only models W2 and W6 gives a good breaking line location. However, the

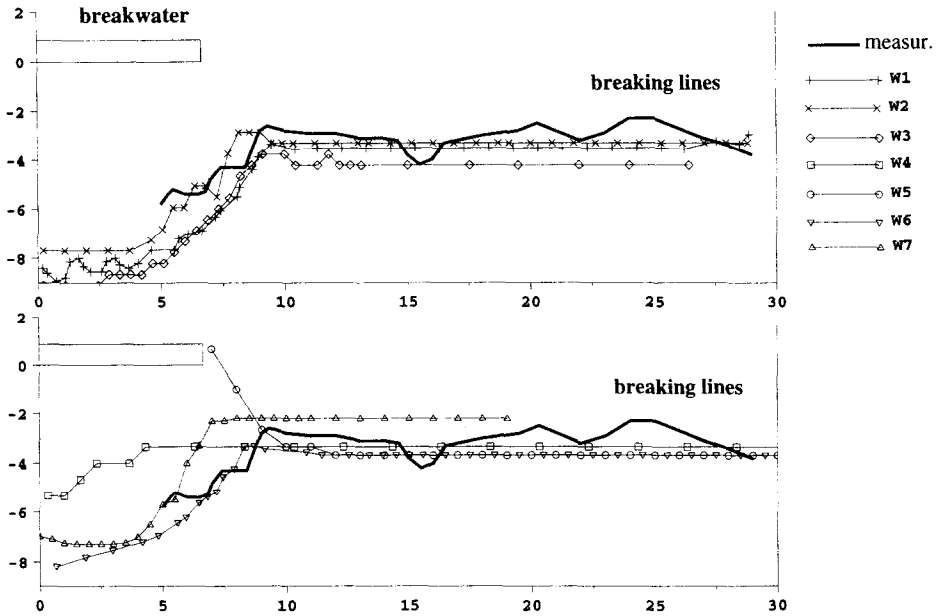


Fig. 2. Measured and computed breaking lines.

deficiencies of the other models in this area should not affect the velocity results since the driving forces are very weak here.

The wave patterns of the numerical models are in qualitative agreement and thus only one is illustrated Fig. 3. The wave height in the cross-shore section  $x = 10$  m (Fig. 4)

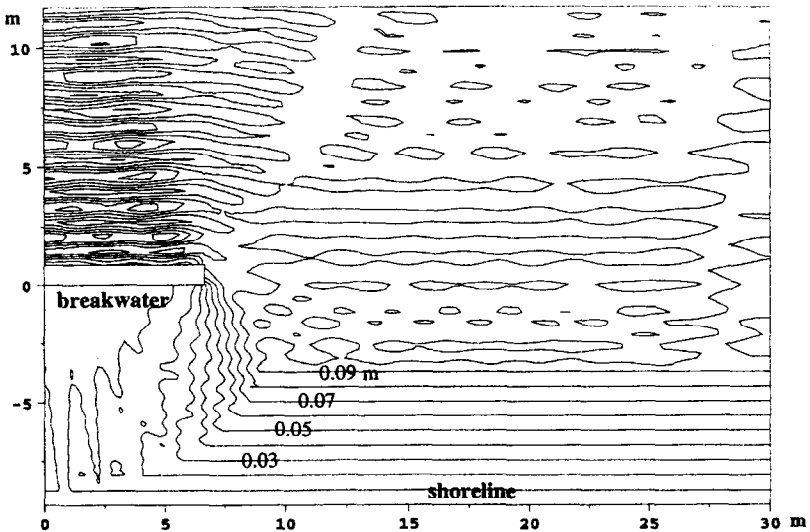


Fig. 3. Computed wave height contour lines — model C1.

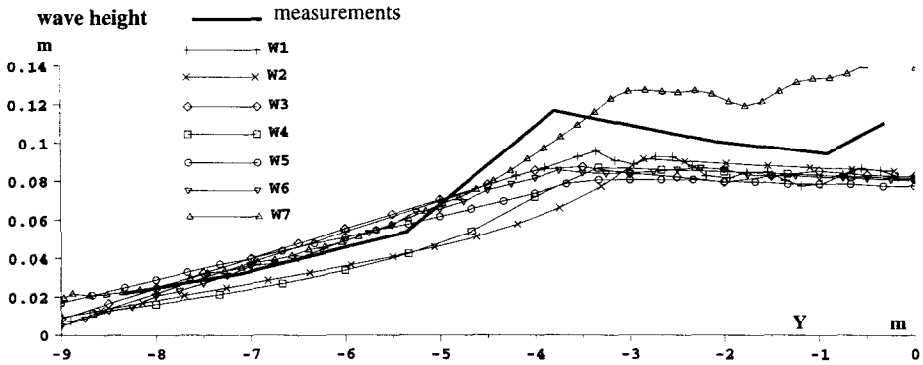


Fig. 4. Computed and measured wave height distribution along profile  $x = 10$  m.

shows that, before the breaking point, the wave models underestimate the wave height, except model W7. The discrepancies between linear wave models and measurements are due to non-linear terms which are not accounted for in linear models. This behaviour was already pointed by some authors (see, e.g., Péchon, 1987).

The wave height decay in the surf zone (Fig. 4) is well represented by numerical models except W2 and W4 where the decay is too pronounced.

#### 4.2. The set-up

Contour lines of set-up computed by C1 are plotted in Fig. 5. In the area not protected by the structure, the driving forces, which are oriented shoreward in the surf-zone, create a set-up of the mean water level and the contour lines are nearly parallel to the shore. Behind the structure the forces are less intense because of smaller wave heights, so the set-up is reduced. The horizontal gradient of mean water level is the only source term of momentum behind the detached breakwater, so a satisfactory reproduction of this factor is fundamental for the modelling of the velocity field.

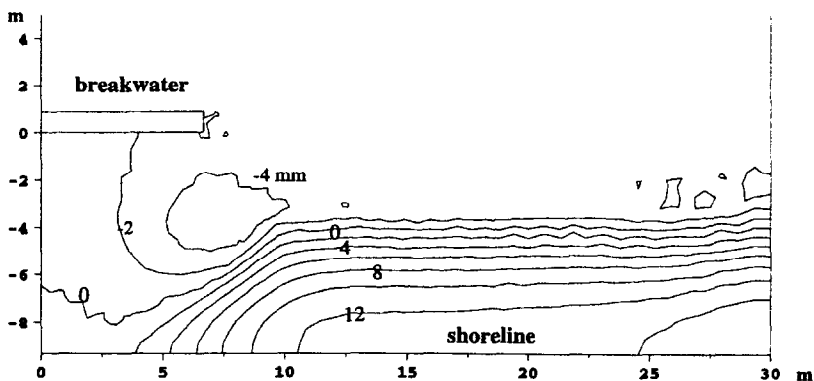


Fig. 5. Computed set-up contour line (in mm) — model C1.

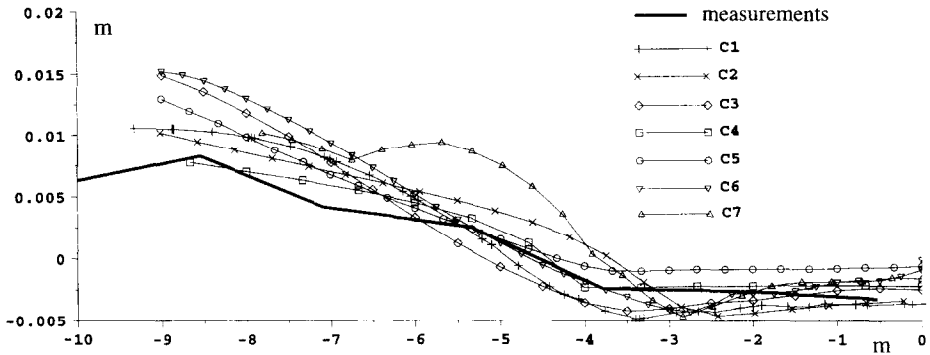


Fig. 6. Computed and measured mean water level along profile  $x = 9$  m.

Fig. 6 displays the computed and measured mean water levels in the cross-shore profile  $x = 9$  m. The measured level in the experimental basin is nearly horizontal and equal to 3 mm between 0 and  $-4$  m and then increases regularly to 8 mm at the shoreline.

The set-up given by models C2 and C4 are in rather good agreement with measurements whereas it is overestimated by other codes. To have a better understanding of the differences, the  $y$ -components of the calculated driving forces which are responsible for cross-shore gradients of the surface level in this section are illustrated on Fig. 7. The distributions of forces are rather different. For example, some curves significantly decrease shoreward (C1, C2, C4 and C7), some are nearly constant (C3 and C6), and one slightly increases (C5).

From Fig. 6, it follows that the expression for the driving forces in terms of wave height always leads to an overestimation of the set-up but this error is compensated in C2 and C4 by an underestimation of the wave height in the profile (see Fig. 4). According to this remark, the driving forces in C1 were multiplied by a coefficient 0.7

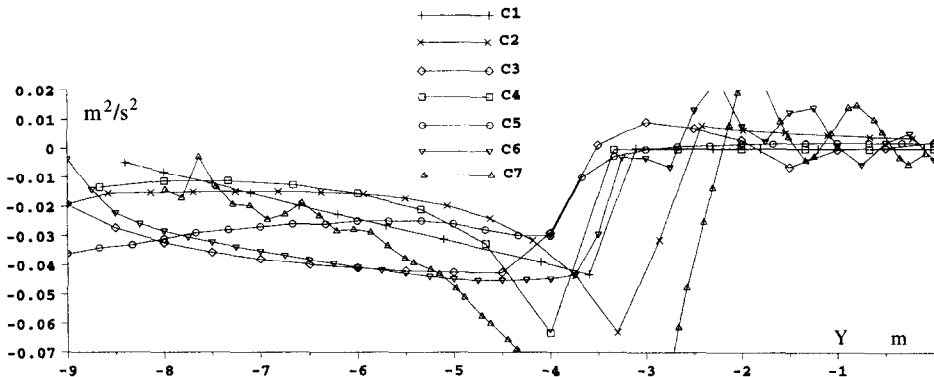


Fig. 7.  $y$ -component of driving force along profile  $x = 10$  m.

as mentioned in Section 2.2.1. It is seen in Fig. 6 that the set-up provided by C1 is closer to measurements at  $x = 9$  m than others models apart from C2 and C4.

#### 4.3. The current field

In the experimental basin, a large eddy was observed behind the detached breakwater (see Fig. 8). Mory and Hamm (1997) pointed out that the velocities were intense along the boundaries limiting the eddy, often over 0.20 m/s, but a wide quiescent region occurred in its centre. Most of the velocity components were measured at mid-depth. However, the velocity distributions along vertical profiles were also collected and the data showed that the horizontal components of velocity were nearly uniform over the water depth in this region.

A large eddy is also reproduced by the seven numerical models. For example, the velocity field computed by C3 is illustrated in Fig. 8; the circulation resulting from other models is in broad qualitative agreement with this pattern. In order to have a deeper insight into differences between models and measurements, velocity vectors in sections  $x = 3$  and 10 m are also plotted in Fig. 9. The velocity vectors in section  $x = 3.0$  m are in reasonable agreement with measurements. In section  $x = 10$  m there are more differences because the dimensions of the simulated eddies are not the same. Moreover in the experimental wave tank, dye tracking displays a contiguous eddy in the open area probably due to longshore irregularities of the generated waves which do not occur in the numerical models.

The quiescent area behind the structure, defined as the region where the velocity is less than 2 cm/s, is shown in Fig. 10. A common behaviour of the numerical results is that the overall water body behind the structure is in rotation and the surface of the quiescent area is at least half as small as the experimental one. A first explanation for this discrepancy could be attributed to an overestimation of the viscosity coefficient in

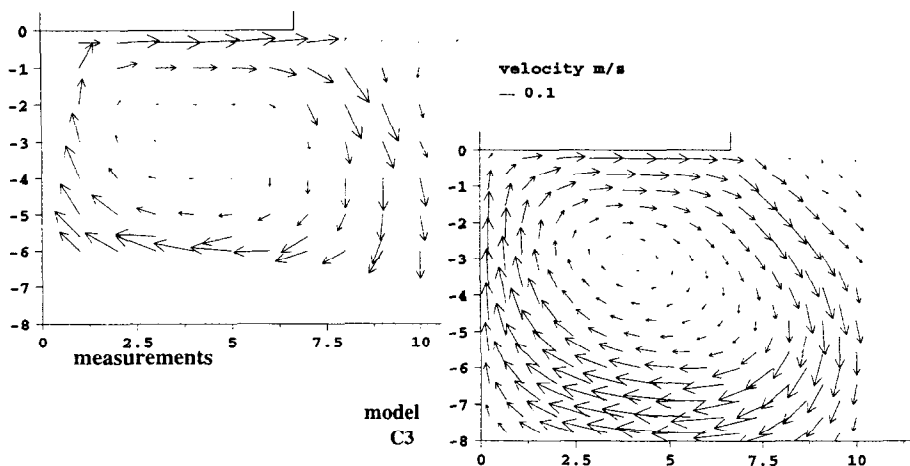


Fig. 8. Measured and computed (model C3) velocity fields behind the structure.

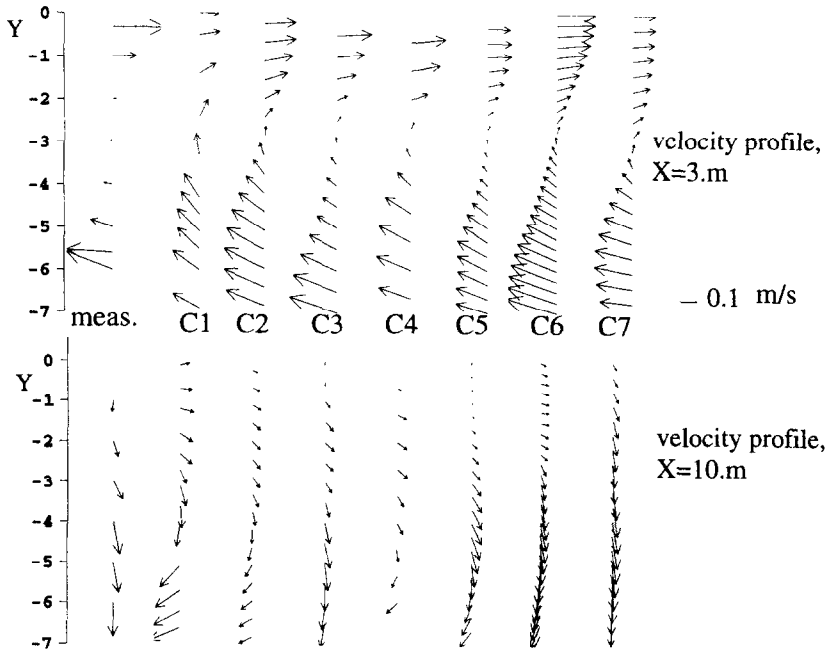


Fig. 9. Measured and computed velocity vectors along profiles  $x = 3$  and  $10$  m.

the numerical models. Distribution of this parameter along the two previous selected profiles is contained in Fig. 11. The sophisticated turbulence models used by C2 and C7 gives strong values in the vicinity of the breaking line and very small values in the section protected by the structure ( $< 0.005 \text{ m}^2/\text{s}$ ); in C5 the viscosity coefficient formulated in local variables is also very small. But in spite of the reduced mixing of

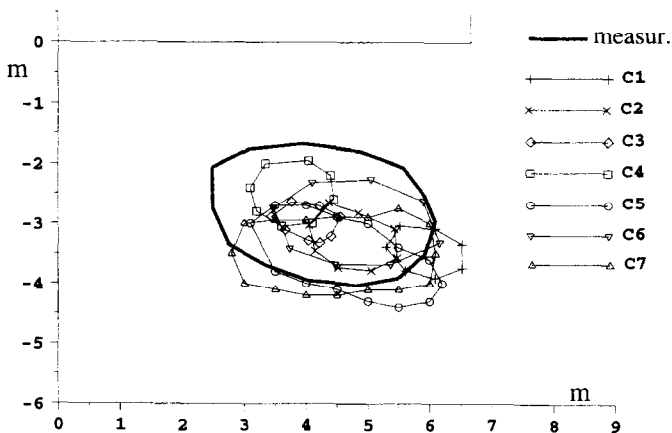


Fig. 10. Computed and measured quiescent areas ( $|\vec{u}| < 0.02 \text{ m/s}$ ) behind the structure.

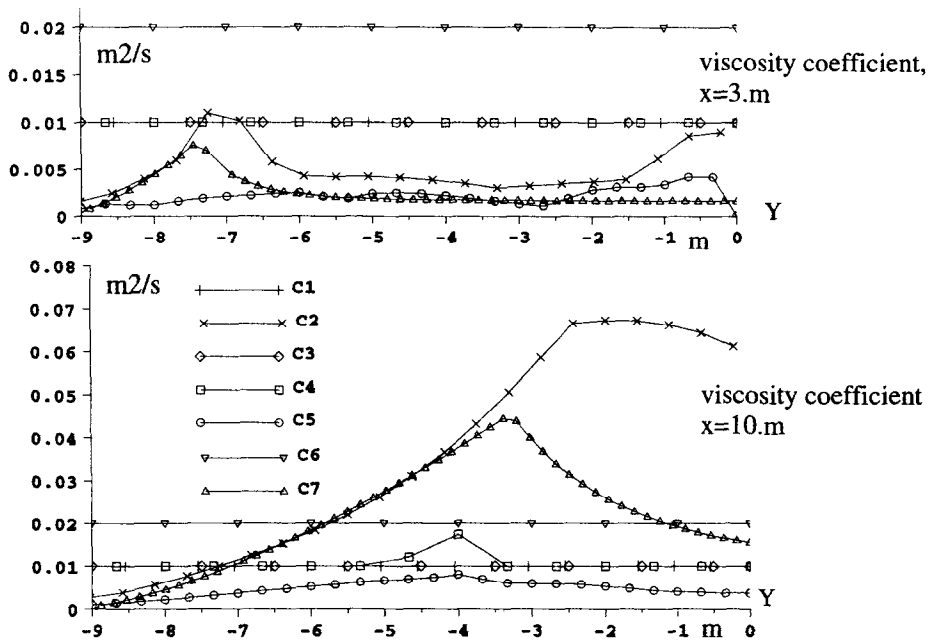


Fig. 11. Viscosity coefficient along profiles  $x = 3$  and  $10$  m.

momentum in the protected area specified in these three models, the simulated quiescent area is too restricted. So this explanation is not sufficient for explaining the differences between measurements and numerical results and another hypothesis will be proposed later in the paper.

The velocity intensity is controlled partly by bottom friction. In order to compare the bed shear stress specified in the models, since the expressions for this term are not equivalent, a friction coefficient  $C$  expressed in  $m^{-1}$  is defined as:

$$C = \tau_b / \rho h u^2$$

where  $\tau_b$  is the modulus of the bottom friction vector;  $u$  is the modulus of the time-averaged velocity vector;  $h$  is the water depth; and  $\rho$  the water density.

It is recalled that all the models take into account wave effects on the bottom shear stress but by different ways (see Section 2.2). The friction coefficient  $C$  is only introduced to allow the comparison between the approaches. This coefficient is plotted in Fig. 12 along the two profiles. For most of the curves, the coefficient increases in a monotonic way with decreasing depth and is smaller in the sheltered area than in the open area. The model C7 leads to higher friction coefficients.

Moreover, it is interesting to note that in C7 the time-averaged bottom stress is not co-linear with the time-averaged velocity. In fact the plot of these two vectors along  $x = 3$  m in Fig. 13 shows that the angle between bottom stress and velocity is  $180^\circ$  in intermediate water depths and is about  $180^\circ + 45^\circ$  near the shoreline. This is an

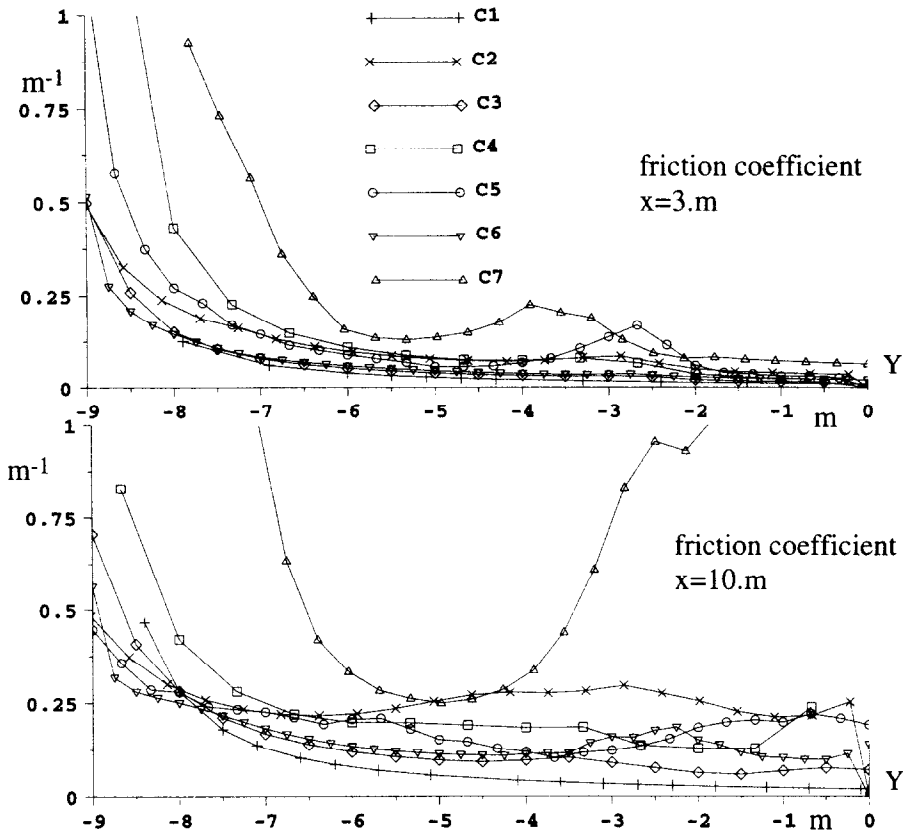


Fig. 12. Friction coefficient along profiles  $x = 3$  and  $10$  m.

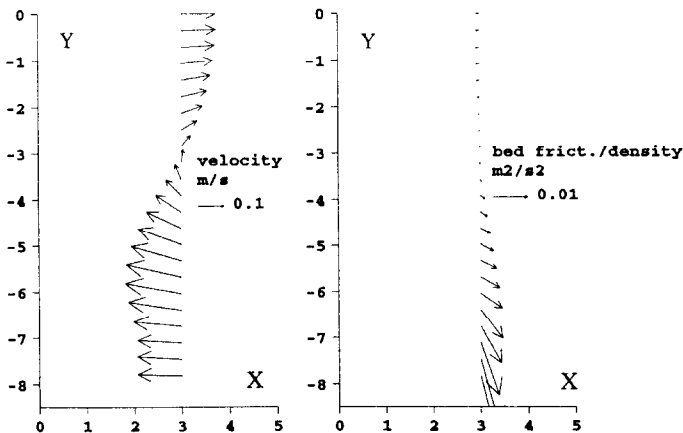


Fig. 13. Comparison of directions of velocity and bed shear stress vectors along profile  $x = 3$  m, model C7.

Table 3  
Mass fluxes between the centre of the eddy and the breakwater

Measurements	C1	C2	C3	C4	C5	C6	C7
$0.042 \pm 0.002$	0.051	0.057	0.056	0.051	0.042	0.061	0.049

important point which can explain the discrepancy concerning the quiescent area in the previous section.

#### 4.4. The mass flux

In order to compare the model results in another way, mass fluxes are integrated along section  $x = 3$  m between the centre of the eddy and the structure. The values expressed in  $\text{m}^3/\text{s}$  are reported in Table 3.

The mass flux produced by C5 agrees closely with the measured value but all the other models overestimate this quantity by more than 25%. This discrepancy is not due to an overestimation of the intensity of velocity along the breakwater but is due to the restricted extent of the quiescent area in the numerical results.

## 5. Conclusions

All the numerical models provide a good prediction of the wave field in the tested situation. However, it is noted that non-linear effects are significant in shallow water and they tend to increase the wave height before breaking. The models are also able to simulate the eddy generated behind the breakwater, but underestimate somewhat the size of the quiescent area at its centre observed in the experimental basin. These results lead to the conclusion that, although significant achievements have been made in the numerical modelling of hydrodynamics in the coastal area, more research on the following items is needed:

- Representation of wave-driven forces. Shortcomings in the modelling of the wave-driven forces have been pointed out; the calculated values seem systematically overestimated. This error is due to the oversimplified description of instantaneous wave orbital velocity in the surf zone.

- Formulation of bed shear stress due to waves and currents. The assumption of co-linearity of the bed shear stress and time-averaged velocity appear to be unrealistic in shallow water.

- Turbulence modelling. The velocity distribution measured in the basin shows that the mixing of momentum due to turbulence is very weak behind the structure in spite of the high turbulent kinetic energy created in the surf-zone and transported by velocities flowing along the shoreline. Even though turbulent parameters were not measured in the basin, the laboratory data indicate that a sophisticated turbulence model is required to represent this effect. Two of the software tested in this paper (C2 and C7) use a transport equation for turbulent kinetic energy. The results display horizontal variations of the turbulent coefficient but the reliability of these turbulence models could not be evaluated in this paper.

Other situations have to be simulated to get experience of models and to draw a complete picture of their performances. The generation of currents driven by irregular waves is also an important item which have to be investigated.

## Acknowledgements

This paper is based on work carried out as part of the G8 Coastal Morphodynamics research programme, in the framework of the EC-sponsored Marine Science and Technology Programme (MAST), under contract No. MAST2-CT92-0027. Much of this work was also co-sponsored by various national funding agencies, among which:

- the Service Central Technique du Secrétariat d'État à la Mer (Compiègne, France),
- the Danish Technical Research Council (STVF),
- the UK Ministry of Agriculture, Fisheries and Food.

The authors are greatly indebted to their colleagues in this project, especially those involved in the working group "Coastal Area Modelling", for their contributions and discussions. They also wish to express their gratitude to those who have made these models operational, and to co-workers and students who have done a significant part of the model running work.

## References

- Battjes, J.A., 1968. Refraction of water waves. *Proc. Am. Soc. Civ. Eng., J. Waterway Harbour Div.*, 94(WW4): 437–451.
- Battjes, J.A., 1975. Modelling of turbulence in the surf-zone. In: *Symposium on Modelling Techniques*. Am. Soc. Civ. Eng., New York, NY, pp. 1050–1061.
- Battjes, J.A. and Janssen, J.P.F.M., 1978. Energy loss and set-up due to breaking of random waves. In: *Proceedings 16th Conference on Coastal Engineering*. Am. Soc. Civ. Eng., New York, NY, pp. 569–587.
- Berkhoff, J.C.W., 1972. Computation of combined effect of currents and underwater topography. In: *Proceedings 13th International Conference on Coastal Engineering*. Am. Soc. Civ. Eng., New York, NY, pp. 471–490.
- Bijker, E.W., 1967. Some considerations about scales for coastal models with movable bed. *Delft Hydraul. Lab., Delft, Publ.* 50.
- Bowen, A.J., 1969. The generation of longshore currents on a plane beach. *J. Mar. Res.*, 27: 206–215.
- Brün, P., 1963. Longshore currents and longshore troughs. *J. Geophys. Res.*, 68: 1065–1078.
- Copeland, G.J.M., 1985a. A practical alternative to mild-slope wave equation. *Coast. Eng.*, 9: 125–149.
- Copeland, G.J.M., 1985b. Practical radiation stress calculations connected with equations of wave propagation. *Coast. Eng.*, 9: 195–219.
- Dally, W.R., Dean, R.G. and Dalrymple, R.A., 1985. A model for breaker decay on beaches. In: *Proceedings 19th Conference on Coastal Engineering*. Am. Soc. Civ. Eng., New York, NY, pp. 82–98.
- de Vriend, H.J. and Stive, M.J.F., 1987. Quasi-3D modelling of nearshore currents. *Coast. Eng.*, 11: 565–601.
- Dingemans, M.W., Radder, A.C. and de Vriend, H.J., 1987. Computation of the driving forces of wave-induced currents. *Coast. Eng.*, 11: 539–563.
- Eagleson, P., 1965. Theoretical study of longshore currents on a plane beach. *Mass. Inst. Technol., Dep. Civ. Eng., Rep. No.* 82.
- Ebersole, B.A. and Dalrymple, R.A., 1979. A numerical modelling for nearshore circulation including convective accelerations and lateral mixing. *Univ. of Delaware, Newark, DE, Ocean Eng. Rep.* 21.
- Fredsoe, J., 1984. The turbulent boundary layer in combined wave-current motion. *Proc. Am. Soc. Civ. Eng., J. Hydraul. Eng.*, 110: 1103–1120.

- Karambas, T.V. and Koutitas, C., 1992. A breaking wave propagation model based on the Boussinesq equations. *Coast. Eng.*, 18(1/2): 1–20.
- Kirby, J.T., 1986. Rational approximations in the parabolic equation method for water waves. *Coast. Eng.*, 10: 355–378.
- Lamb, H., 1932. *Hydrodynamics*. Cambridge University Press, London, 738 pp.
- Longuet Higgins, M.S., 1970. Longshore currents generated by obliquely incident sea waves. *J. Geophys. Res.*, 75(33): 203–248.
- Mory, M. and Hamm, L., 1997. Wave, set-up and currents around a detached breakwater submitted to regular or random wave forcing. *Coast. Eng.*, 31: 77–96.
- Nicholson, J., Tanguy, J.-M., Roelvink, J.A., Price, D., Broker, I. and Moreno, L., 1997. Intercomparison of coastal area morphodynamic models. *Coast. Eng.*, 31: 97–123.
- Nishimura, H., 1982. Numerical simulation of nearshore circulations. In: *Proceedings 29th Japanese Conference on Coastal Engineering*. Jpn. Soc. Civ. Eng., Tokyo, pp. 333–137 (in Japanese).
- Péchon, P., 1987. Modelling of longshore currents with a non-linear theory. In: *Proceedings of the Coastal Hydrodynamics Conference*. Am. Soc. Civ. Eng., New York, NY, pp. 170–183.
- Péchon, P. and Teisson, C., 1995. Numerical modelling of three-dimensional wave-driven currents in the surf-zone. In: *Proceedings 24th Conference on Coastal Engineering*. Am. Soc. Civ. Eng., New York, NY, pp. 2503–2512.
- Putnam, D.A., Munk, W.H. and Traylor, M.A., 1949. The production of longshore currents. *Trans. Am. Geophys. Union*, pp. 337–345.
- Rivero, F.J. and Arcilla, A.S., 1993. Propagation of linear gravity waves over slowly varying depth and currents. *Proc. Waves'93 Symp.*, pp. 518–532.
- Rivero, F.J. and Arcilla, A.S., 1995. On the vertical distribution of  $\langle \tilde{u}\tilde{w} \rangle$ . *Coast. Eng.*, 25: 137–152.
- Sanchez-Arcilla, A., Collado, F. and Rodriguez, A., 1992. Vertically varying velocity field in 3D nearshore circulation. In: *Proc. 22th Conference on Coastal Engineering*. Am. Soc. Civ. Eng., New York, NY, pp. 2811–2824.
- Soulsby, R.L., Hamm, L., Klopman, G., Myrhaug, D., Simons, R.R. and Thomas, G.P., 1993. Wave-current interaction within and outside the bottom boundary layer. *Coast. Eng.*, 21: 41–69.
- Southgate, H.N., 1989. A nearshore profile model of wave and tidal current interaction. *Coast. Eng.*, 13: 219–246.
- Svendsen, J.A. and Lorentz, R.S., 1989. Velocities in combined undertow and longshore currents. *Coast. Eng.*, 13: 55–79.
- Swart, D.H., 1974. *Offshore sediment transport and equilibrium beach profiles*. Delft Hydraul. Lab., Delft, Publ. 131.
- Wind, H.G. and Vreugdenhil, C.B., 1986. Rip-current generation near structures. *J. Fluid Mech.*, 171: 459–476.
- Wu, C.S. and Liu, P.L.F., 1982. Finite element modelling of breaking wave induced nearshore current. In: T.K. Kawai (Editor), *Finite Element Flow Analysis*. pp. 579–586.
- Yoo, D. and O'Connor, B.A., 1986. Mathematical modelling of wave-induced nearshore circulations. In: *Proceedings 20th International Conference on Coastal Engineering*. Am. Soc. Civ. Eng., New York, NY, pp. 1667–1682.
- Yoo, D. and O'Connor, B.A., 1988a. Turbulence transport modelling of wave-induced currents. In: B.A. Schreffer and O.C. Zienkiewicz (Editors), *Computed Modelling in Ocean Engineering*. A.A. Balkema, Rotterdam, pp. 151–158.
- Yoo, D. and O'Connor, B.A., 1988b. Mean bed friction of combined wave current flow. *Coast. Eng.*, 12: 1–21.